

# RSC Advances



This is an *Accepted Manuscript*, which has been through the Royal Society of Chemistry peer review process and has been accepted for publication.

*Accepted Manuscripts* are published online shortly after acceptance, before technical editing, formatting and proof reading. Using this free service, authors can make their results available to the community, in citable form, before we publish the edited article. This *Accepted Manuscript* will be replaced by the edited, formatted and paginated article as soon as this is available.

You can find more information about *Accepted Manuscripts* in the [Information for Authors](#).

Please note that technical editing may introduce minor changes to the text and/or graphics, which may alter content. The journal's standard [Terms & Conditions](#) and the [Ethical guidelines](#) still apply. In no event shall the Royal Society of Chemistry be held responsible for any errors or omissions in this *Accepted Manuscript* or any consequences arising from the use of any information it contains.

Cite this: DOI: 10.1039/c0xx00000x

www.rsc.org/xxxxxx

ARTICLE TYPE

# Preparation of novel flower-like MnO<sub>2</sub>/BiOI composite with highly enhanced adsorption and photocatalytic activity

Suqin Liu\*, Huizhen Liu, Guanhua Jin, Hao Yuan

*Received (in XXX, XXX) Xth XXXXXXXXX 20XX, Accepted Xth XXXXXXXXX 20XX*

DOI: 10.1039/b000000x

A novel flower-like MnO<sub>2</sub>/BiOI composite has been fabricated by a simple and cost-effective approach. Multiple experiments are carried out to optimize the molar ratio of MnO<sub>2</sub>/BiOI for the decomposition of methyl orange (MO) and Rhodamine B (RhB). The adsorption property of as-prepared samples in dark condition and photocatalytic activity under visible light and simulated solar light irradiation are investigated in detail. When the MnO<sub>2</sub>/BiOI molar ratio is 4 : 5, the highest photocatalytic activity for degradation of MO (97.8%) and RhB (91.7%) is achieved under visible light irradiation for 40 min as well as simulated solar light irradiation (93.4% for MO and 88.2% for RhB within 40 min). The excellent photocatalytic performances are attributed to the synergistic effect of BiOI and MnO<sub>2</sub> and the unique flower-like morphology of MnO<sub>2</sub>/BiOI composite as verified by relative experiments.

## 1. Introduction

The toxicity and carcinogenicity of colored dyes to humans in environment are the major concerns all the time.<sup>1</sup> As the well-known typical dyes, methyl orange (MO) and Rhodamine B (RhB) are widely used in textiles, printings, papers, foods, pharmaceutical industries and research laboratories.<sup>2,3</sup> Therefore, more and more efforts have been made to explore efficient treatment strategies for their degradation.<sup>4-10</sup>

Semiconductor photocatalysis is of great potential to decompose organic water pollutants into CO<sub>2</sub> and H<sub>2</sub>O using solar light.<sup>7, 11-13</sup> As a representative of traditional photocatalytic materials, TiO<sub>2</sub> is widely studied by virtues of its nontoxicity, high chemical stability, low cost and outstanding oxidative power.<sup>14</sup> However, TiO<sub>2</sub> could only respond to ultraviolet radiation because of its large band gap (3.0-3.2 eV), which leads to low photocatalytic efficiency. Recently, bismuth oxyhalides (BiOX, X = F, Cl, Br, and I) with layered structures have been put forward as promising candidate photocatalysts under both ultraviolet and visible light irradiation.<sup>6, 15, 16</sup> Among them, BiOI exhibited the best photocatalytic activity because of its smallest band gap (1.77-1.92 eV).<sup>15, 17, 18</sup> Even so, the photocatalytic activity of BiOI has been still restricted by some disadvantages, such as low efficiency of light absorption, slow rate of charge transfer and high recombination probability of the photogenerated electron-hole pairs.<sup>19, 20</sup> In the past few years, coupling with second semiconductors, such as Bi<sub>2</sub>S<sub>3</sub>/BiOI,<sup>6</sup> AgI/BiOI,<sup>18</sup> ZnO/BiOI,<sup>21</sup> TiO<sub>2</sub>/BiOI,<sup>22</sup> BiOI/BiOX,<sup>23-25</sup> and MnO<sub>x</sub>-BiOI,<sup>26</sup> has been proposed to notably reduce the recombination possibility and accelerate the separation rate of photogenerated charge carriers, thus effectively improve the photodegradability of semiconductor oxide photocatalyst. As a result, an increasing number of studies have focused on the coupled semiconductor

systems.

MnO<sub>2</sub> is of considerable importance in technological applications including electrochemical supercapacitor, molecular adsorption, catalysis and ion-exchange due to its masses of merits like inexpensive, non-toxic and ease of fabrication. As a typical catalyst, MnO<sub>2</sub> is extensively investigated for oxidation of organic pollutants in wastewater because of its strong adsorption and oxidation ability.<sup>9, 27-30</sup> Dong et al. found that MnO<sub>2</sub> possesses high adsorption capacity to MO with a removal efficiency of 78.6%.<sup>28</sup> It is reported that MnO<sub>2</sub> has a narrow band gap of 0.25 eV, which enable it to absorb the light at infrared wavelengths in theory and increase the utilization rate of solar energy when combination with other type photocatalyst such as TiO<sub>2</sub>.<sup>31-33</sup> Recently, to improve the photocatalytic activity of BiOI, MnO<sub>x</sub> is considered as a deriving-hole-type cocatalyst to enhance the transfer of the photo-induced holes.<sup>26</sup> Ye et al. reported that MnO<sub>x</sub>-BiOI can deliver higher photocatalytic activity than BiOI for the degradation of RhB dye under visible light irradiation. However, the reported highest photocatalytic degradation efficiency of the prepared MnO<sub>x</sub>-BiOI *via* photo-deposition method for RhB under visible light in 30 min is only 78.8%.<sup>26</sup>

As is well known, the photocatalytic activity is much depended on the morphology, fabrication strategy and the component of cocatalyst. In general, the catalyst with a morphology which has larger surface area, trends to show better photocatalytic activities due to the masses of exposed active sites. In addition, the combination structure also remarkably affects the photocatalytic performance. Based on these, in this manuscript, a novel flower-like MnO<sub>2</sub>/BiOI hybrid composite is fabricated by a simple two-step method. And the catalytic activity of MnO<sub>2</sub>/BiOI composites with different molar ratio is investigated by decomposing MO and RhB under dark condition, visible light and simulated solar

light irradiation at room temperature. As expected, the as-prepared MnO<sub>2</sub>/BiOI composite demonstrates much higher photocatalytic activity than the bare BiOI and MnO<sub>2</sub>. Furthermore, the possible reasons and photocatalytic mechanism have been put forward based on the investigation of reactive species.

## 2. Experimental

### 2.1 Preparation of catalyst

All the reagents were analytically pure and used as received without further purification. The NaI was bought from Aladdin Chemistry Co., Ltd. Other chemicals were purchased from Sinopharm Chemical Reagent Co., Ltd.

In a typical experiment, 316 mg of KMnO<sub>4</sub> was dissolved in 112 mL of deionized water by strong magnetic stirring. Then, 11 mL of 6 mol L<sup>-1</sup> HCl solution was slowly dropped into the previous solution under stirring. The as-obtained MnO<sub>2</sub> precipitates were collected by centrifugation, after washing several times with distilled water and ethanol and dried in an oven overnight at 60 °C finally.

The pure BiOI was synthesized according to ref. 34. 0.728 g of Bi(NO<sub>3</sub>)<sub>3</sub>·5H<sub>2</sub>O was added in 20 mL of absolute ethanol under stirring at room temperature for 30 min. Then, 40 mL of NaI solution (0.225 g of NaI dissolved in distilled water) was added dropwise into the previous solution. The pH of the mixture was adjusted to 7 by adding 1.5 mol · L<sup>-1</sup> NH<sub>3</sub>H<sub>2</sub>O. Then, the mixture was transferred to a 250 mL flask and maintained at 80 °C for 3 h by oil bath heating. After completion of the reaction, the precipitates were collected by centrifugation, washed several times with distilled water and ethanol and dried in an oven overnight at 60 °C finally.

In order to synthesize MnO<sub>2</sub>/BiOI composite, the as-prepared MnO<sub>2</sub> was well dispersed by ultrasound for 1 hour in ethanol solution containing the same molar of Bi(NO<sub>3</sub>)<sub>3</sub>·5H<sub>2</sub>O. The subsequent operations are the same as the preparation of BiOI. For comparison, MnO<sub>2</sub>/BiOI composites with molar ratio of MnO<sub>2</sub> to Bi(NO<sub>3</sub>)<sub>3</sub>·5H<sub>2</sub>O (2/7, 3/5, 4/5, 4/4, 6/3) are designed.

### 2.2 Characterization

The crystal phases of the samples were analyzed by a MXP-AHF X-ray diffractometer from 10° to 80° with a Cu Kα of 1.54056 Å. Scanning electron microscopy (SEM, JEOL JSM-6360) and high-resolution transmission electron microscopy (HRTEM, JEOL JEM-2010) were employed to observe the morphologies and microstructures. The Brunauer-Emmett-Teller (BET) surface area was measured using a Quantachrome autosorb-1 automated gas sorption systems at 77K. X-ray photoelectron spectroscopy (XPS) was measured with a Thermo VG Scientific Sigma Probe spectrometer. A Perkin-Elmer Optima-8000 was used to determine the real amount of MnO<sub>2</sub> and BiOI in the samples by inductively coupled plasma analysis (ICP). The UV-VIS diffuse reflection spectra were obtained for the dry-pressed disk samples using a Scan UV-VIS spectrophotometer (UV-VIS DRS : UV-2550, Shimadzu) equipped with an integrating sphere assembly, using BaSO<sub>4</sub> as reflectance sample.

### 2.3 Photocatalytic experiments

The photocatalytic activities were evaluated by the photodegradation of MO and RhB under the irradiation of dark, visible light and simulated sunlight, respectively. The pH value was not adjusted when the reaction was conducted. Experiments were carried out at room temperature. A 300 W Xe lamp (PLS-SXE300, Beijing Trusttech Co., Ltd.) equipped with a 400 nm cutoff filter was used as the visible light source, and the distance between the liquid surface of the suspension and the light source was set about 20 cm. A 150 W solar simulator (Beijing Zolix Instrument CO., Ltd.) was used as the simulated sunlight source, and the distance between the liquid surface of the suspension and the light source was set about 15 cm. The photodegradation experiments were carried out with the sample power (100 mg) suspended in MO or RhB solution (100 mL, 10 mg L<sup>-1</sup>) with constant stirring. Prior to irradiation, the suspensions were magnetically stirred in the dark for 30 min to obtain the desorption-adsorption equilibrium. A magnetic stirrer was employed for continuous mixing during the dark and visible light excluding simulated solar light irradiation. At certain time intervals, 10 mL suspensions were sampled and centrifuged to remove the particles. For catalytic MO and RhB degradation, each experiment was repeated three times in order to obtain error bars on the plots. The filtrates of MO and RhB degradation were analyzed by a UV-vis spectro-photometer (UV-1780, Shimadzu) at wavelength 464 nm and 574 nm, respectively.

## 3. Results and discussion

### 3.1 Characterization of MnO<sub>2</sub>/BiOI

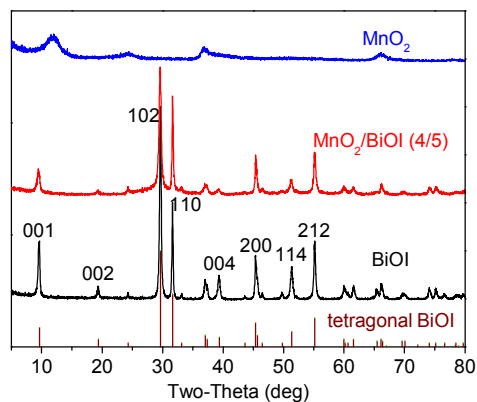


Fig. 1 XRD patterns of the as-prepared BiOI, MnO<sub>2</sub>/BiOI (4/5), and MnO<sub>2</sub>

Fig.1 presents the XRD patterns of the pure BiOI, MnO<sub>2</sub> and MnO<sub>2</sub>/BiOI (4/5). All the diffraction peaks of the bare BiOI could be well assigned to the tetragonal phase (JCPDS card no. 10-0445).<sup>35</sup> The three diffraction peaks at  $2\theta = 29.3^\circ$ ,  $31.8^\circ$  and  $45.6^\circ$  are well assigned to the (102), (110) and (200) planes of BiOI, respectively. The sharp and narrow diffraction peaks indicate that the sample is well crystallized. The XRD peaks of MnO<sub>2</sub> match well with the layered birnessite-type MnO<sub>2</sub> (JCPDS card no. 80-1098).<sup>36</sup> The low intensity reveals the poor crystallinity of the MnO<sub>2</sub>. The MnO<sub>2</sub>/BiOI composite (4/5) shows similar diffraction

lines to that of the pure BiOI, and no obvious diffraction lines of  $\text{MnO}_2$  is observed. This may be due to the low diffraction intensity of  $\text{MnO}_2$ . Meanwhile, the main peak of  $\text{MnO}_2$  is very close to that of BiOI. Similar phenomenon was observed in previous literatures.<sup>26, 33</sup>

To further confirm the existence of  $\text{MnO}_2$  in the composite, X-ray photoemission spectroscopy (XPS) (Fig. 2) is applied to investigate the surface composition and chemical state of the  $\text{MnO}_2/\text{BiOI}$  (4/5) composite and the physical mixed  $\text{MnO}_2$  and BiOI (marked as  $\text{MnO}_2 + \text{BiOI}$  (4 + 5)). Elements of Bi, O, I and Mn are clearly observed in the survey spectra (Fig. 2a). The high resolution XPS of Mn 2p<sub>3/2</sub> is displayed in Fig. 2b, from which two peaks positioned at 642.2 eV and 654.2 eV, which are ascribed to the Mn 2p<sub>3/2</sub> state and Mn 2p<sub>1/2</sub>, are observed.<sup>26</sup> The two strong peaks at 159.0 eV and 164.4 eV in the high resolution XPS of Bi 4f (Fig. 2c) are assigned to Bi 4f<sub>7/2</sub> and Bi 4f<sub>5/2</sub> peaks of Bi<sup>3+</sup>, in good agreement with the valence state of Bi in BiOI.<sup>26</sup> As shown in Fig. 2d, the two peaks of I region at 619.0 eV and 630.5 eV relate to the I 3d<sub>5/2</sub> and I 3d<sub>3/2</sub>, respectively, corresponding to the characteristics of I in the BiOI. The O1s core level spectrum (Fig. 2e) of  $\text{MnO}_2/\text{BiOI}$  (4/5) could be fitted to three peaks at 529.7 eV, 530.4 eV and 531.8 eV,<sup>26</sup> which could be assigned to the Mn-O-Mn<sup>37</sup> bonds in  $\text{MnO}_2$ , Bi-O bonds<sup>22</sup> in [Bi<sub>2</sub>O<sub>2</sub>] slabs of BiOI layered structure, and hydroxyl groups, respectively. Note that the peaks of Mn-O-Mn bonds and Bi-O bonds in  $\text{MnO}_2/\text{BiOI}$  (4/5) has a slight shift compared with those of physical sample  $\text{MnO}_2 + \text{BiOI}$  (4+5) (Fig. 2f), implying the interaction between  $\text{MnO}_2$  and BiOI.

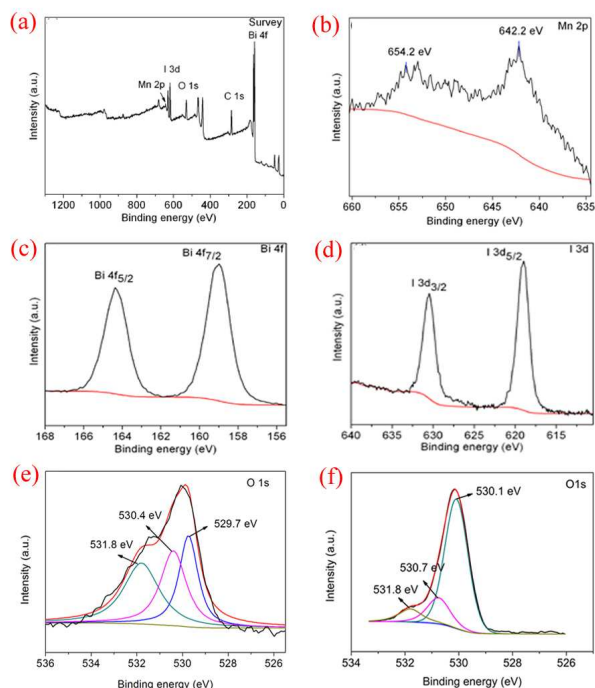


Fig. 2 The survey XPS of  $\text{MnO}_2/\text{BiOI}$  (4/5) (a), high resolution XPS of Mn 2p (b), Bi 4f (c), I 3d (d), O 1s (e) in  $\text{MnO}_2/\text{BiOI}$  (4/5), and O 1s (f) in  $\text{MnO}_2 + \text{BiOI}$  (4+5)

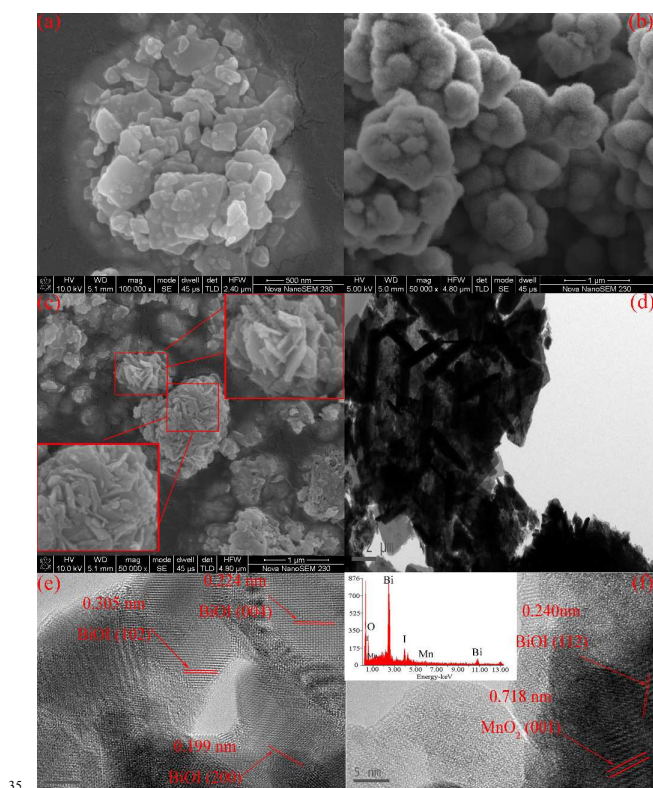


Fig. 3 SEM images of BiOI (a) and  $\text{MnO}_2$  (b); SEM (c), TEM (d) and HRTEM (d, f) images of  $\text{MnO}_2/\text{BiOI}$  (4/5) composite; Inset is EDS image of  $\text{MnO}_2/\text{BiOI}$  (4/5) composite.

The morphology features of the as-prepared products were characterized by SEM, TEM, and HRTEM. Fig. 3a shows that the pure BiOI is composed of smooth flakes with uneven size less than 500 nm. The pure  $\text{MnO}_2$  is of microsphere with a diameter of 500 nm, but an aggregation takes place (Fig. 3b). The  $\text{MnO}_2/\text{BiOI}$  (4/5) composite demonstrates a flower-like morphology structure, which is constructed by many straight flakes (Fig. 3c and d). The diameter of the flower is about 1  $\mu\text{m}$ , reveal a possible combination of  $\text{MnO}_2$  and BiOI. Note that, in the preparation process, the  $\text{MnO}_2$  was dispersed in the  $\text{Bi}(\text{NO}_3)_3$  solution by ultrasound firstly. Then, I was added. After adjusting the pH to 7, the primary BiOI crystals were formed firstly and prefer to grow in the surface of  $\text{MnO}_2$  when precipitating from solution owing to the tendency to reduce the total surface energy. As a result, a different flower-like morphology was formed. In such a unique flower-like structure, the BiOI could contact with  $\text{MnO}_2$  intimately, which will facilitate the fast transfer of photo-induced carriers. Additionally, as seen from the TEM picture (Fig. 3d), the flakes stack and intercross with one another, forming a lot of pores in the surface. The abundant voids could not only enrich the active sites of BiOI, but also increase the contact between catalyst and MO solution, which will benefit to the photocatalytic activity.

The HRTEM images of the  $\text{MnO}_2/\text{BiOI}$  composite are given in Fig. 3d and Fig. 3e. Three sets of different fringes are clearly found. The fringe spacing of 0.305 nm, 0.224 nm and 0.199 nm agree well with the spacing of the (102), (004) and (200) lattice planes of BiOI, respectively. In Fig. 3e, lattice fringes with

spacing of 0.240 nm and 0.718 nm are found, corresponding to the (112) facet of BiOI and the (001) facet of MnO<sub>2</sub>, respectively.<sup>38</sup> The well-defined fringes and the high crystallinity of the MnO<sub>2</sub>/BiOI composite will facilitate the separation of the photo-induced carrier and thus improve the corresponding catalytic activities.<sup>18</sup> In the EDS image (Fig. 3f inset), elements of Mn, I, Bi and O are clearly displayed, further confirming the co-existence of MnO<sub>2</sub> and BiOI.

### 3.2 Optical absorption properties

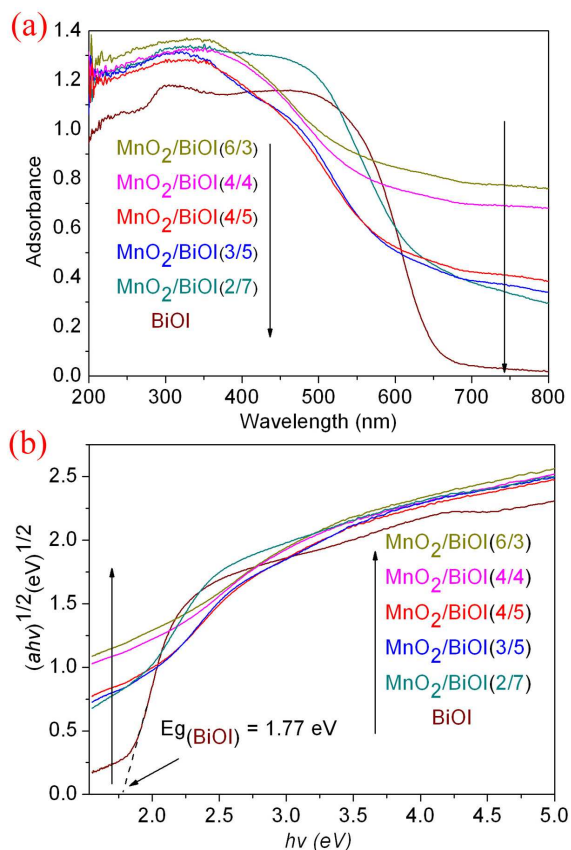


Fig. 4 (a) UV-Vis diffuse reflectance spectra (DRS) of as-prepared MnO<sub>2</sub>/BiOI samples; (b) the plotting of  $(ah\nu)^{1/2}$  vs. photon energy

The optical absorption and energy band feature of a semiconductor are crucial factors determining its photocatalytic performance. Fig. 4 is the UV-vis DRS of the as-prepared samples. As seen, BiOI has a strong absorption edge for visible light at about 650 nm. Increasing the MnO<sub>2</sub> content, the absorption edge of MnO<sub>2</sub>/BiOI shows an obvious red shift. Meanwhile, the absorption intensity of MnO<sub>2</sub>/BiOI is enhanced gradually. The band gap energy of a semiconductor could be calculated by the following formula:<sup>5, 18, 39</sup>

$$ah\nu = A(h\nu - E_g)^{n/2} \quad (1)$$

where  $\alpha$ ,  $\nu$ ,  $E_g$ , and  $A$  are the absorption coefficient, light frequency, band gap, and a constant, respectively. Among them,  $n$  depends on the characteristics of the transition in a semiconductor, including direct transition ( $n = 1$ ) or indirect transition ( $n = 4$ ). The indirect band gaps are obtained from the intersection of the plot of  $[ah\nu]^{1/2}$  versus  $h\nu$ . For the pure BiOI,

the indirect band gap ( $E_g$ ) is estimated to be 1.77 eV, in good accordance with the band gap of BiOI previously reported.<sup>5, 17, 40</sup>

Although the band edge positions of the BiOI are not easily determined experimentally, a theoretical prediction is possible using concepts of electronegativity. The conduction band (CB) and valence band (VB) potentials can be calculated by the following equations:<sup>41</sup>

$$E_{VB} = X - E^c + 0.5 E_g \quad (2)$$

$$E_{CB} = E_{VB} - E_g \quad (3)$$

Where  $E_{VB}$  is the VB edge potential,  $E_{CB}$  is the CB edge potential,  $X$  is the electronegativity of the semiconductor, which can be calculated as the geometric mean of the electronegativity of the constituent atoms. The  $X$  value for BiOI is *ca.* 5.99 eV according to relative reports.<sup>5</sup>  $E^c$  is the energy of free electrons on the hydrogen scale (about 4.5 eV),  $E_g$  is the band gap energy (1.77 eV) of the semiconductor. Accordingly, the VB and CB of BiOI were estimated to be 2.38 and 0.61 eV, respectively. Because the band edges could move with the change of pH value, the new potentials of VB and CB for BiOI at pH = 7.0 is calculated according to Eq. (4):<sup>42-44</sup>

$$E_{fp} = E_{fp}^0 - 0.05915 pH \quad (4)$$

Where  $E_{fp}^0$  is the flat band potential of catalyst when the pH is 0.

When the pH is 7.0, the corresponding VB and CB of BiOI are 1.97 and 0.20 eV, respectively.

### 3.3 Catalytic activity of MnO<sub>2</sub>/BiOI

MO and RhB were chosen as different types of model pollutants to evaluate the adsorption ability and photocatalytic activity of the as-prepared samples under dark condition and visible light irradiation, respectively. Fig. 5 shows that the concentration of dyes declines gradually without visible light irradiation, which is attributed to the adsorption process.<sup>5, 6, 9, 35</sup> The pure BiOI shows negligible activity for MO or RhB adsorption. By contrast, about 57.2% of MO and 40.3% of RhB are adsorbed by MnO<sub>2</sub> after 30 min, illustrating relative strong sorption ability. When the molar ratio of MnO<sub>2</sub> to BiOI is 4/5, the highest adsorption performance of both MO and RhB are achieved. This phenomenon may have a relationship with their special BET surface areas ( $S_{BET}$ ). The  $S_{BET}$  of the pure BiOI, MnO<sub>2</sub> and MnO<sub>2</sub>/BiOI (4/5) composite are 13.19, 32.72 and 47.38 m<sup>2</sup> g<sup>-1</sup>, respectively. It is well accepted that the large specific surface area will be beneficial to the adsorption ability.<sup>23</sup> Obviously, the largest  $S_{BET}$  of MnO<sub>2</sub>/BiOI (4/5) composite origins from its special flower-like structure, in which amount of voids exist.

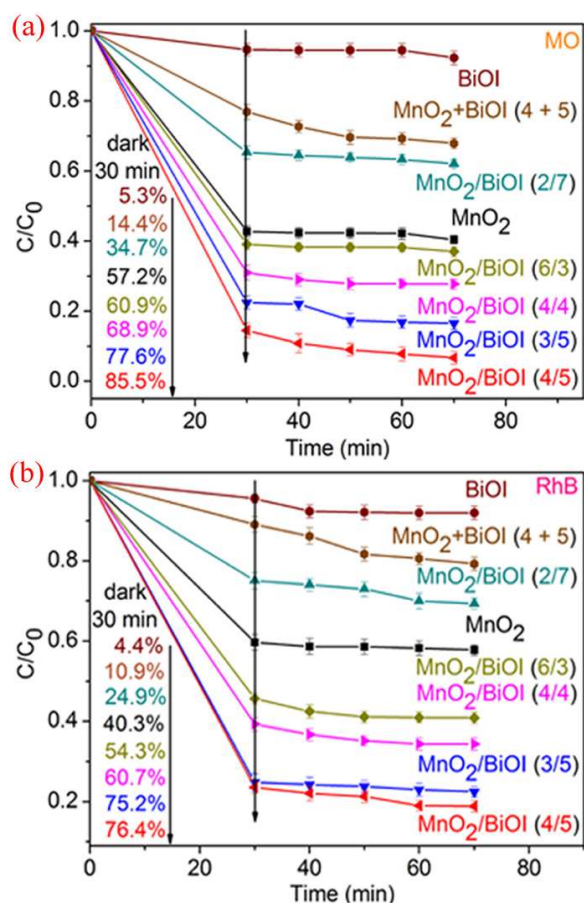


Fig. 5 Adsorption of MO (a) and RhB (b) as a function of time under dark condition

As seen from the adsorption data, the concentration of the MO and RhB solution shows negligible decrease after 30 min in the darkness. Therefore, we irradiated the samples with visible or simulated solar light after treating the solution under dark conditions for 30 min. As shown in Fig. 6a and Fig. 6b, the concentration of dyes decrease slightly in the absence of catalyst, which confirm the good chemical stability of MO and RhB. For MnO<sub>2</sub>, about 60.5% of MO and 43.4% of RhB are removed in 40 min under visible light irradiation, closing to its adsorption capacity (59.5% for MO and 42.2% for RhB). The poor photocatalysis activity may have relationship with its narrow band gap of 0.25 eV, which enable it to absorb the light at infrared wavelengths.<sup>31-33</sup> It is worth noting that, the photocatalytic conversion of MO degradation over the MnO<sub>2</sub>/BiOI (4/5) sample reach the max value of 94% after just 10 min irradiation. As is shown in Fig. 6c, the main peak of MO ( $\lambda = 464$  nm) completely disappears only after 10 min irradiation. Moreover, the color of the supernatant changes from yellow to colorless observed by the naked eye, verifying the excellent photocatalytic activity of the MnO<sub>2</sub>/BiOI (4/5) under visible light irradiation. Such result is much higher than that of the bare BiOI (44.4% in 10 min). Significantly, the as-obtained MnO<sub>2</sub>/BiOI (4/5) also shows a relatively high photocatalytic performance for RhB with a degradation ratio of 91.7% after 40 min of visible light

irradiation. At the same time, it can be seen from Fig. 6d that most the fuchsia color of the starting RhB solution fades just after visible light irradiation for 10 min. And an evident decrease from 2.109 to 0.083 in RhB absorption at  $\lambda = 554$  nm is observed. Obviously, the MnO<sub>2</sub>/BiOI (4/5) composite demonstrates much enhanced catalytic activity than the bare BiOI and MnO<sub>2</sub>. The highest photocatalytic activity of MnO<sub>2</sub>/BiOI (4/5) is mainly attributed to the synergistic effect between MnO<sub>2</sub> and BiOI. It was reported that MnO<sub>2</sub> could act as a deriving-hole type cocatalyst to enhance the separation efficiency of the photoinduced carriers of BiOI.<sup>26</sup> The detailed photocatalytic mechanisms are further discussed in the photocatalytic mechanism part. Moreover, the unique flower-like morphology will also contribute to the outstanding photocatalytic performance. In this structure, the intimate conduct contact between MnO<sub>2</sub> and BiOI is conducive to the charge transfer from BiOI to MnO<sub>2</sub>. This could be confirmed by the low photocatalytic activities of the physical mixed MnO<sub>2</sub> and BiOI (marked as MnO<sub>2</sub> + BiOI (4 + 5)) under both dark condition and visible light irradiation. Note that a simple physical mixing could not provide a close combination of MnO<sub>2</sub> and BiOI, thus the charge transfer is not fluent.<sup>5, 20</sup> In addition, the flower-like morphology has a relative high S<sub>BET</sub> which increase the surface active sites as well as the contact area between the dye solution and catalyst.<sup>1, 45, 46</sup>

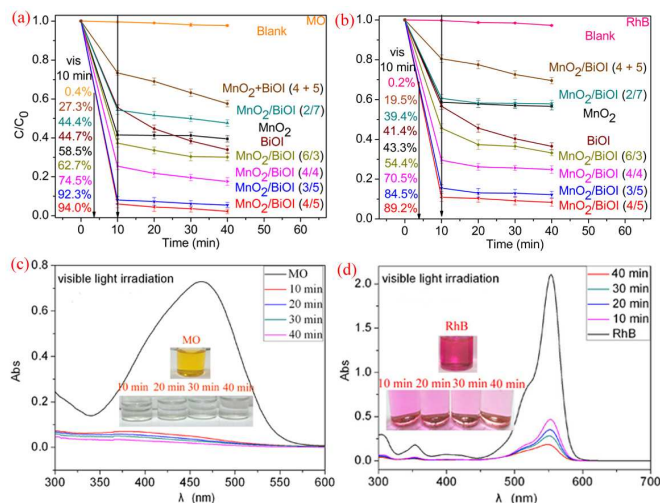


Fig. 6 Photodegradation of MO (a) and RhB (b) as a function of irradiation time; UV-Vis spectral changes of MO (c) and RhB (d) as a function of irradiation time over MnO<sub>2</sub>/BiOI (4/5)

To further reveal the excellent photocatalytic performance of the MnO<sub>2</sub>/BiOI (4/5) composite, we also evaluated the photocatalytic activity using MO and RhB under simulated solar light irradiation. As Fig. 7 displayed, the highest photocatalytic activity is still achieved over the MnO<sub>2</sub>/BiOI (4/5) sample, inducing 93.4% for MO and 88.2% for RhB degradation within 40 min. The cause of the slight decrease in activity for the MnO<sub>2</sub>/BiOI(4/5) sample compared to the degradation performance (97.8% for MO and 91.7% for RhB) under visible light is that the photodegradation experiments under simulated solar light irradiation were performed without constant stirring.

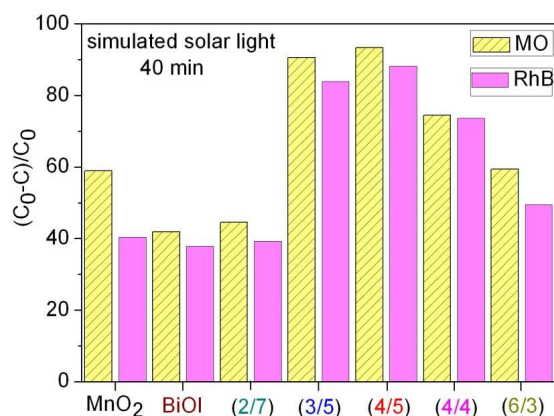


Fig. 7 Photocatalytic activity of the bare MnO<sub>2</sub>, BiOI, and MnO<sub>2</sub>/BiOI samples with different molar ratios (MnO<sub>2</sub>/BiOI) under simulated solar light irradiation

### 3.4 Possible photocatalytic mechanism

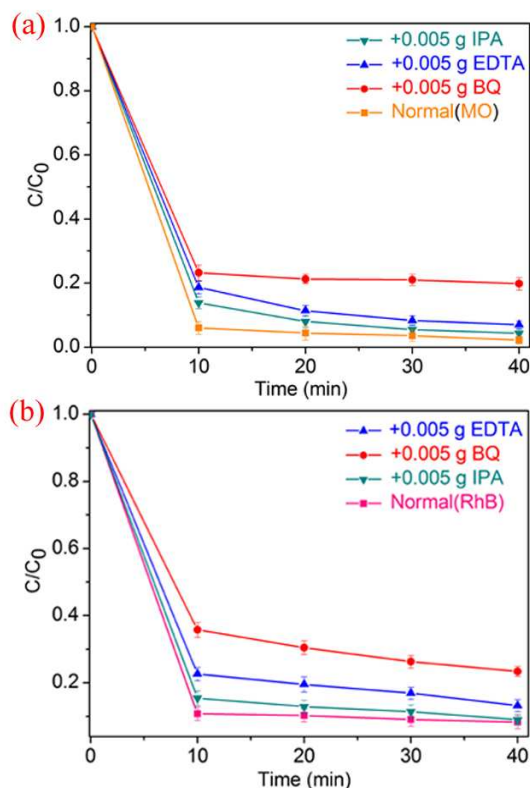


Fig. 8 Effects of different scavengers on the degradation of MO (a) and RhB (b) over MnO<sub>2</sub>/BiOI (4/5) composite

As is well known, during the photocatalytic oxidation (PCO) process, a series of reactive oxygen species, such as  $h^+$ ,  $\cdot OH$ , or  $\cdot O_2^-$ , are supposed to be involved. In order to investigate the roles of these reactive species, we conducted the reactive species trapping experiments. In our experiments, isopropanol (IPA),<sup>47, 48</sup> ethylene diamine tetraacetic acid (EDTA),<sup>5, 49</sup> and benzoquinone (BQ),<sup>50, 51</sup> acting as the scavengers for  $\cdot OH$ ,  $h^+$  and  $\cdot O_2^-$ , are introduced into the PCO process, respectively.

Fig. 8 shows the variation of MO and RhB degradation with different quenchers. Both the MO and RhB solution added with

IPA affect the photocatalytic activity of MnO<sub>2</sub>/BiOI (4/5) slightly, suggesting that  $\cdot OH$  does not play a key role for the degradation of the two dyes. On the contrary, the photocatalytic degradation of MO or RhB is obviously inhibited after the addition of BQ or EDTA, which implies that  $h^+$  and  $\cdot O_2^-$  played major role in MnO<sub>2</sub>/BiOI (4/5) under visible light irradiation. This corresponds well with the previous reported results.

Based on above results, the coupling effects of MnO<sub>2</sub> and BiOI was proposed to explain the enhanced photocatalytic activity of MnO<sub>2</sub>/BiOI (4/5) composite. The proposed schematic mechanism of MnO<sub>2</sub>/BiOI composite is shown in Fig. 9. It is well known that the photodegradation processes are depended on charge carrier generation and separation. As shown in Fig. 9, under visible excitation, the electron of BiOI can be promoted from the valence band to the conduction band, leaving behind a hole in the valence band. Then the photoinduced holes transfer to MnO<sub>2</sub> and largely reduce the recombination of photogenerated electrons and holes, thus more effective electrons and holes are taking part in the photodegradation process.<sup>26</sup>

The unique flower-like morphology of the composite also attributes to the remarkable photocatalytic performance. Firstly, the relative high  $S_{BET}$  and massed of pores increase the surface active sites as well as the contact area between the dye solution and catalyst. Moreover, the enhanced sensitization effect between the dyes and BiOI may also be beneficial to the degradation efficiency. In the process of dye photosensitization, the electrons on the highest occupied molecular orbital (HOMO) of dye molecules will be excited to the lowest unoccupied molecular orbitals (LUMO) under visible light, and subsequently would be injected to the CB of BiOI. Then the adsorbed molecular oxygen would capture the electrons in the CB of BiOI to form  $\cdot O_2^-$  radicals, which degrade the adsorbed MO or RhB dye further.<sup>5, 6</sup> That is why the  $\cdot O_2^-$  scavenger suppresses dye degradation as shown in Fig. 8. At the same time, the photoinduced holes on the surface of BiOI can also directly oxidize the organic pollutants. That is to say, the photocatalytic process and photosensitization process jointly involve in the dye degradation.

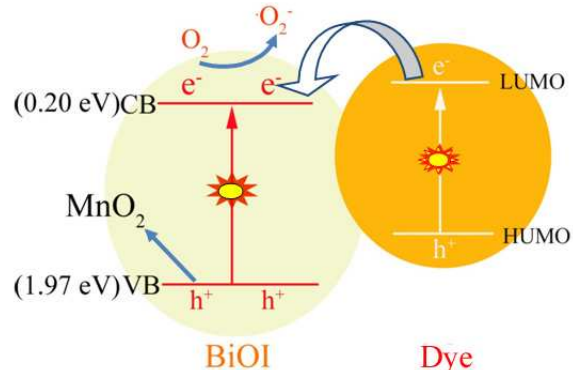


Fig. 9 The proposed possible mechanism for the improvement of photocatalytic activity

## 4. Conclusion

In summary, we report a simple, economical and effective synthesis of a novel flower-like MnO<sub>2</sub>/BiOI composite. The optimum MnO<sub>2</sub>/BiOI composite (4/5) demonstrate a maximal photocatalytic degradation efficiency of 97.8% under visible light

and 93.4% under simulated solar light irradiation for MO within 40 min. In addition, the RhB removal efficiency reached 91.7% and 88.2% in 40 min under visible and simulated solar light irradiation, respectively. The outstanding photocatalytic activity is attributed to the cocatalytic effect of MnO<sub>2</sub> and BiOI, as well as the unique flower-like morphology, which provide a relative high S<sub>BET</sub> and intimate contact of MnO<sub>2</sub> and BiOI. Our results suggest that MnO<sub>2</sub>/BiOI composites may be promising photocatalyst for the degradation of organic pollutants due to its low cost and super-photocatalytic performance under visible light.

## Notes and references

<sup>a</sup> Address, Address, Town, Country. Fax: XX XXXX XXXX; Tel: XX XXXX XXXX; E-mail: xxx@aaa.bbb.ccc

1. W. Dong, C. W. Lee, X. Lu, Y. Sun, W. Hua, G. Zhuang, S. Zhang, J. Chen, H. Hou and D. Zhao, *Appl. Catal., B*, 2010, **95**, 197-207.
2. A. Mittal, A. Malviya, D. Kaur, J. Mittal and L. Kurup, *J. Hazard. Mater.*, 2007, **148**, 229-240.
3. Z. Ai, Y. Wang, M. Xiao, L. Zhang and J. Qiu, *J. Phys. Chem. C*, 2008, **112**, 9847-9853.
4. L. Zhou, C. Gao and W. Xu, *ACS Appl. Mater. Inter.*, 2010, **2**, 1483-1491.
5. T. B. Li, G. Chen, C. Zhou, Z. Y. Shen, R. C. Jin and J. X. Sun, *Dalton Trans.*, 2011, **40**, 6751-6758.
6. J. Cao, B. Xu, H. Lin, B. Luo and S. Chen, *Dalton Trans.*, 2012, **41**, 11482-11490.
7. J. Cao, X. Li, H. Lin, S. Chen and X. Fu, *J. Hazard. Mater.*, 2012, **239**, 316-324.
8. S. Li, Z. Ma, L. Wang and J. Liu, *Sci. China, Ser. B: Chem.*, 2008, **51**, 179-185.
9. H. Zhao, G. Zhang and Q. Zhang, *Ultrason. Sonochem.*, 2014, **21**, 991-996.
10. J. Di, J. Xia, S. Yin, H. Xu, L. Xu, Y. Xu, M. He and H. Li, *J. Mater. Chem. A*, 2014, **2**, 5340-5351.
11. A. Fujishima, *Nature*, 1972, **238**, 37-38.
12. M. Su, C. He, L. Zhu, Z. Sun, C. Shan, Q. Zhang, D. Shu, R. Qiu and Y. Xiong, *J. Hazard. Mater.*, 2012, **229**, 72-82.
13. M. R. Hoffmann, S. T. Martin, W. Choi and D. W. Bahnemann, *Chem. Rev.*, 1995, **95**, 69-96.
14. J. Sun, X. Li, Q. Zhao, J. Ke and D. Zhang, *J. Phys. Chem. C*, 2014.
15. X. Zhang, Z. Ai, F. Jia and L. Zhang, *J. Phys. Chem. C*, 2008, **112**, 747-753.
16. J. Henle, P. Simon, A. Frenzel, S. Scholz and S. Kaskel, *Chem. Mater.*, 2007, **19**, 366-373.
17. X. Chang, J. Huang, C. Cheng, Q. Sui, W. Sha, G. Ji, S. Deng and G. Yu, *Catal. Commun.*, 2010, **11**, 460-464.
18. H. Cheng, B. Huang, Y. Dai, X. Qin and X. Zhang, *Langmuir*, 2010, **26**, 6618-6624.
19. L. Zhao, Z. Liu, X. Zhang, T. Cui, J. Han, K. Guo, B. Wang, Y. Li, T. Hong, J. Liu and Z. Liu, *RSC Adv.*, 2014, **4**, 45540-45547.
20. J. Di, J. Xia, S. Yin, H. Xu, L. Xu, Y. Xu, M. He and H. Li, *J. Mater. Chem. A*, 2014, **2**, 5340-5351.
21. J. Jiang, X. Zhang, P. Sun and L. Zhang, *J. Phys. Chem. C*, 2011, **115**, 20555-20564.
22. Y. Zhang, S. Liu, Z. Xiu, Q. Lu, H. Sun and G. Liu, *J. Nanopart. Res.*, 2014, **16**, 1-9.
23. F. Dong, Y. Sun, M. Fu, Z. Wu and S. Lee, *J. Hazard. Mater.*, 2012, **219**, 26-34.
24. X. Xiao, R. Hao, M. Liang, X. Zuo, J. Nan, L. Li and W. Zhang, *J. Hazard. Mater.*, 2012, **233**, 122-130.
25. J. Cao, B. Xu, H. Lin, B. Luo and S. Chen, *Chem. Eng. J.*, 2012, **185**, 91-99.
26. L. Ye, X. Liu, Q. Zhao, H. Xie and L. Zan, *J. Mater. Chem. A*, 2013, **1**, 8978-8983.
27. G. Fu, H. E. Allen and C. E. Cowan, *Soil Sci.*, 1991, **152**, 72-81.
28. W. F. Dong, L. H. Zang and H. Li, *Appl. Mech. Mater.*, 2013, **361**, 760-763.
29. D. Zhao, X. Yang, H. Zhang, C. Chen and X. Wang, *Chem. Eng. J.*, 2010, **164**, 49-55.
30. M. Singh, D. N. Thanh, P. Ulbrich, N. Strnadová and F. Štěpánek, *J. Solid State Chem.*, 2010, **183**, 2979-2986.
31. Z. Zou, Y. Liu, H. Li, Y. Liao and C. Xie, *J. Comb. Chem.*, 2010, **12**, 363-369.
32. L. Zhang, D. He and P. Jiang, *Catal. Commun.*, 2009, **10**, 1414-1416.
33. M. Xue, L. Huang, J.-Q. Wang, Y. Wang, L. Gao, J.-H. Zhu and Z.-G. Zou, *Nanotechnology*, 2008, **19**, 185604.
34. X. Xiao and W.-D. Zhang, *J. Mater. Chem.*, 2010, **20**, 5866-5870.
35. Y. Park, Y. Na, D. Pradhan, B.-K. Min and Y. Sohn, *CrystEngComm*, 2014, **16**, 3155-3167.
36. Y. Wang, H. Sun, H. M. Ang, M. O. Tade and S. Wang, *Appl. Catal., B*, 2015, **164**, 159-167.
37. Z. Lei, F. Shi and L. Lu, *ACS Appl. Mater. Inter.*, 2012, **4**, 1058-1064.
38. F. Zhou, H. Zheng, X. Zhao, Q. Guo, X. Ni, T. Shen and C. Tang, *Nanotechnology*, 2005, **16**, 2072.
39. M. Butler, *J. Appl. Phys.*, 1977, **48**, 1914-1920.
40. Y. Wang, K. Deng and L. Zhang, *J. Phys. Chem. C*, 2011, **115**, 14300-14308.
41. X. Zhang, L. Zhang, T. Xie and D. Wang, *J. Phys. Chem. C*, 2009, **113**, 7371-7378.
42. M. Hepel and J. Luo, *Electrochim. Acta*, 2001, **47**, 729-740.
43. J. M. Bolts and M. S. Wrighton, *J. Phys. Chem.*, 1976, **80**, 2641-2645.
44. D. Chen and A. K Ray, *Chem. Eng. Sci.*, 2001, **56**, 1561-1570.
45. J. Zhao, T. Wu, K. Wu, K. Oikawa, H. Hidaka and N. Serpone, *Environ. Sci. Technol.*, 1998, **32**, 2394-2400.
46. Y. Shiraishi, N. Saito and T. Hirai, *J. Am. Chem. Soc.*, 2005, **127**, 12820-12822.
47. L.-S. Zhang, K.-H. Wong, H.-Y. Yip, C. Hu, J. C. Yu, C.-Y. Chan and P.-K. Wong, *Environ. Sci. Technol.*, 2010, **44**, 1392-1398.
48. Y. Chen, S. Yang, K. Wang and L. Lou, *J. Photochem. Photobiol., A*, 2005, **172**, 47-54.
49. L. M. Pastrana-Martínez, J. L. Faria, J. M. Doña-Rodríguez, C. Fernández-Rodríguez and A. M. Silva, *Appl. Catal., B*, 2012, **113**, 221-227.
50. J. Bandara and J. Kiwi, *New J. Chem.*, 1999, **23**, 717-724.
51. M. Yin, Z. Li, J. Kou and Z. Zou, *Environ. Sci. Technol.*, 2009, **43**, 8361-8366.